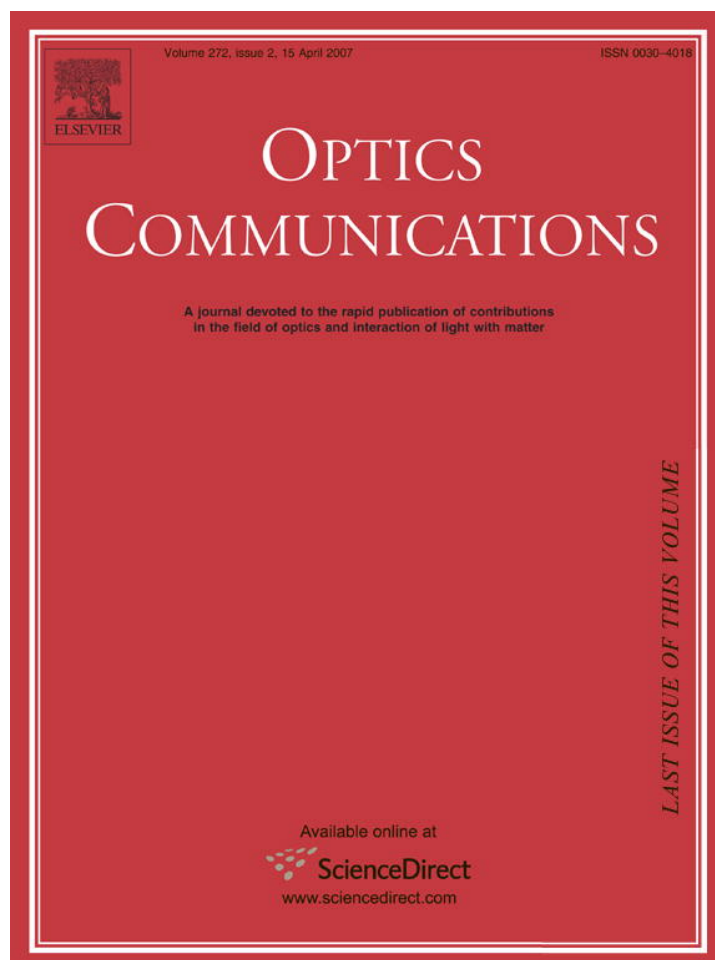


Provided for non-commercial research and educational use only.  
Not for reproduction or distribution or commercial use.



This article was originally published in a journal published by Elsevier, and the attached copy is provided by Elsevier for the author's benefit and for the benefit of the author's institution, for non-commercial research and educational use including without limitation use in instruction at your institution, sending it to specific colleagues that you know, and providing a copy to your institution's administrator.

All other uses, reproduction and distribution, including without limitation commercial reprints, selling or licensing copies or access, or posting on open internet sites, your personal or institution's website or repository, are prohibited. For exceptions, permission may be sought for such use through Elsevier's permissions site at:

<http://www.elsevier.com/locate/permissionusematerial>



# EIT at $5^2S_{1/2} \rightarrow 6^2P_{3/2}$ transition in a mismatched V-type rubidium system

Silvije Vdović \*, Ticijana Ban, Damir Aumiler, Goran Pichler

*Institute of physics, Bijenička 46, 10000 Zagreb, Croatia*

Received 22 September 2006; accepted 30 November 2006

## Abstract

Induced transparency on a blue probe light in a Doppler broadened V-type mismatched system using a low power near infrared coupling diode laser was experimentally observed. Extensive theoretical model was used which utilizes the three-level V-type scheme. Appropriate modifications were made to take into account the hyperfine splitting of the ground  $5^2S_{1/2}$  and excited  $5^2P_{3/2}$  and  $6^2P_{3/2}$  states. Calculated probe absorption line profiles reproduce with great accuracy measured absorption profiles. The influence of the  $5^2P_{3/2}$ – $6^2P_{3/2}$  unlinked states coherence on the induced transparency was discussed in the context of the used theoretical model.

© 2006 Elsevier B.V. All rights reserved.

PACS: 42.50.Gy; 32.80.Qk; 42.50.Nn

## 1. Introduction

Quantum coherence and interference among atomic states coupled by laser field provide a variety of phenomena for fundamental and practical applications. Electromagnetically induced transparency (EIT) is a phenomenon of induced transparency in an initially absorbing medium, experienced by a weak probe field due to the presence of the strong coupling field [1,2]. It was first discussed theoretically by Imamoglu and Harris [3] and for the first time experimentally observed in neutral strontium [4]. Since then, several theoretical EIT descriptions in different atomic systems appeared, followed by corresponding experimental observations. EIT is a main driving force for the phenomena like lasing without inversion (LWI) [5,6], slow light generation [7] (phaseonium-type media), enhancement of non-linear wave-mixing [7,8], quantum information storage [9], magneto-optical switch [10], etc.

The light amplification and the lasing without inversion have been the subject of substantial experimental work due to the possibility of generating laser light at regions of the electromagnetic spectrum which are not conventionally accessible. Several experiments have demonstrated non-inversion amplification in the  $\Lambda$ -type systems [6,11]. However,  $\Lambda$ -type systems involve coherent population trapping and these effects can be understood as an amplification with inversion in a dressed state basis picture. The first observation of continuous wave inversionless lasing was demonstrated by Zibrov and co-workers [12]. Their scheme utilized almost matched (equal probe and coupling field frequency) three-level Rb atom in a V-type configuration. V-type LWI presents the cancellation of absorption caused by the quantum interference without any hidden inversion in a dressed state basis.

Mismatched (unequal probe and coupling field frequency) V-type systems with coupling field frequency lower than the probe field frequency are ideal candidates for the high-frequency inversionless laser systems [13]. On that

\* Corresponding author. Tel.: +385 14698858; fax: +385 14698889.  
E-mail address: [silvije@ifs.hr](mailto:silvije@ifs.hr) (S. Vdović).

account, the study of electromagnetically induced transparency in such systems represents the first step in a high-frequency inversionless lasers realization. EIT creates the reduction in absorption upon which the LWI is based. Additionally, the V-type configuration provides optimal transparency in the Doppler-broadened systems, particularly for the cases in which the probe frequency is much larger than the coupling field frequency [13,14]. Therefore, the EIT investigation in the Doppler broadened mismatched V-type system could provide new insights for other inhomogeneously broadened media such as quantum wells. The first and unique experimental observation of cw mismatched transparency in a V-type Doppler broadened system was presented by Boon et al. [15]. These authors produced the transparency on the  $5^2S_{1/2} \rightarrow 6^2P_{1/2}$  transition (blue line at 422 nm) by the application of the near infrared coupling laser on the  $5^2S_{1/2} \rightarrow 5^2P_{3/2}$  transition (780 nm). Using the coupling field power of 800 mW, corresponding to the Rabi frequency of 2.2 GHz, they obtained the induced transparency on  $^{85}\text{Rb } F_g = 2 \rightarrow F_c = 1, 2, 3$  transition (422 nm) which removes 73% of the absorption.

Up to now it has been thought that mismatched wavelength systems subjected to Doppler broadening can only be realized for high coupling powers [16]. In the present paper, we investigate the EIT in the Rb mismatched V-type Doppler broadened system using the low power coupling field. Our atomic system is similar to the one in Ref. [15]. The transparency is induced on a weak blue 420 nm probe field ( $5^2S_{1/2} \rightarrow 6^2P_{3/2}$  transition) by application of a 780 nm coupling field. For coupling field power of only 35 mW, we obtained the induced transparency on  $^{85}\text{Rb } F_g = 2 \rightarrow F_c = 1, 2, 3$  transition which removes 67% of the absorption in a peak of the Doppler broadened line profile. Due to the low coupling field power, most of the induced transparency is a result of the ground  $5^2S_{1/2}(F_g = 2)$  level population decrease induced by the coupling field saturation effect.

We performed standard but very elaborate density matrix analysis, which enabled to distinguish between the coherent and incoherent mechanisms responsible for the observed transparency.

## 2. Experiment

A simplified experimental scheme is presented in Fig. 1. The rubidium vapor was generated in a 5 mm long T-shaped all sapphire cell (ASC) containing pure rubidium. The cell was heated in the specially designed oven to increase the atom number density. This enables measurable absorption at 420 nm probe transition, which has a small transition dipole moment. The optimal absorption cancellation was observed for the vapor temperature of about 110 °C. The dominant mechanism for the absorption cancellation at lower vapor temperatures is the optical pumping of the ground state hyperfine levels, which masks the EIT signal. At higher vapor temperatures, increased optical

thickness on coupling transition is limiting the observation of EIT signal.

Coupling and probe laser fields were supplied from two current and temperature stabilized cw external cavity diode laser systems (TOPTICA DL100) with a linewidth of about 1 MHz. The coupling and the probe fields propagated collinearly. In this way, for an atom velocity group the Doppler shifts of the coupling laser and probe laser are partially cancelled. This configuration can reduce the requirement for the coupling intensity to create effective atomic coherence [17]. The residual two-photon Doppler linewidth [14] at 110 °C is about 300 MHz. The overlap of coupling and probe beams was optimized using the dichroic mirror DM1. The beams of approximately the same size were focused by a lens with focal length of 45 cm, giving the beam waist of about 100  $\mu\text{m}$  in the centre of the cell. The coupling field of 50 mW maximum output power was tuned to  $^{85}\text{Rb } 5^2S_{1/2} \rightarrow 5^2P_{3/2}$  transition at 780 nm. Its wavelength was stabilized using Doppler-free saturated absorption spectroscopy [18], providing negligible frequency drift during the measurements. The probe beam frequency was scanned across the hyperfine structure of the  $^{85}\text{Rb } 5^2S_{1/2} \rightarrow 6^2P_{3/2}$  transition region with a 0.23 GHz/ms scanning rate. The relevant energy level structure of  $^{85}\text{Rb}$  isotope is shown in Fig. 2. The probe field power was about 10  $\mu\text{W}$ . The available coupling field power was 35 mW, which gives an estimated Rabi frequency of 500 MHz. The Rabi frequency is calculated using the  $5^2S_{1/2} \rightarrow 5^2P_{3/2}$  transition dipole moment [19] and coupling beam profile in the centre of the cell. After passing through the cell the two beams were separated with a dichroic mirror DM2. The probe beam was directed through the Schott BG18 filter (in order to reduce any residual coupling laser signal) to the photodiode, and detected at the oscilloscope (HAMEG HM1507-3).

## 3. Theory

Theoretical modeling was carried out utilizing a three-level V scheme with appropriate modifications to take into account the hyperfine splitting of the  $^{85}\text{Rb } 5^2S_{1/2}$  ground and  $5^2P_{3/2}$ ,  $6^2P_{3/2}$  excited states. A system of 55 coupled differential equations for the slowly varying density-matrix elements in the 10-level scheme of  $^{85}\text{Rb}$  was obtained. Additional terms were included in the equations to account for the repopulation of the ground states due to spontaneous decay from the excited states (repopulation terms) and the thermalization of the hyperfine ground and excited levels (collisional mixing term). The repopulation terms were calculated from the appropriate radiative decay rates  $\Gamma_{ij}^{\text{rad}}$ . The collisional mixing term  $\Pi$  was calculated from the collisional cross section [20], average atom velocity and the atomic number density. In our experimental conditions, it amounts to about 12 MHz, which is fast enough to prevent optical pumping of the ground hyperfine levels.

The coherence decay rates ( $\gamma_{ij}$ ) were calculated according to the relation:

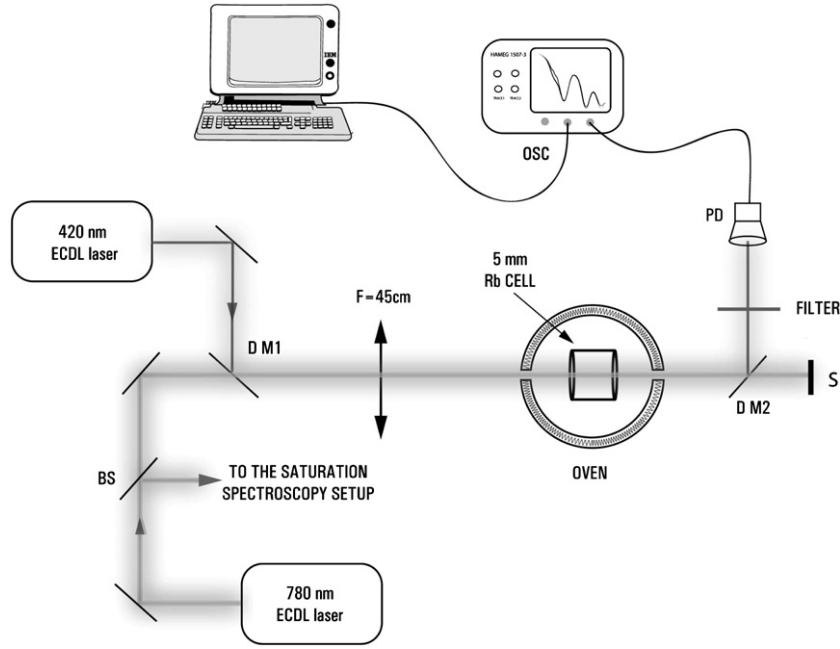


Fig. 1. Experimental scheme: PD-photodiode, BS-beam splitter, DM1 and DM2-dichroic mirrors, S-beam stopper.

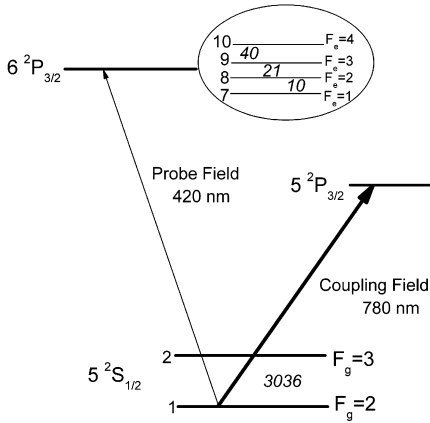


Fig. 2. Energy-level picture of the V scheme employed in  $^{85}\text{Rb}$  isotope including hyperfine splittings of ground  $5^2\text{S}_{1/2}$  and excited  $5^2\text{P}_{3/2}$ ,  $6^2\text{P}_{3/2}$  states. The ground and excited hyperfine energy separations are given in MHz. The states are denoted by numbers starting with the state of lowest energy.

$$\gamma_{ij} = \frac{1}{2} (\Gamma_i^{\text{tot}} + \Gamma_j^{\text{tot}}). \quad (1)$$

$\Gamma_i^{\text{tot}}$  denotes total decay rate of atomic level  $i$  ( $i = 1, 2, \dots, 10$ , see Fig. 2). It is a sum of radiative and collisional decay rates. Collisional decay rates include inelastic collision decay rates and elastic collision decay rates. Inelastic collisions contribute to the population and coherence decay and in our model they are included through the thermalization process with inelastic decay rate equal to  $\Pi$ . On the other hand, elastic collisions do not cause population decay, they only contribute to the decay of coherence. Total decay rates  $\Gamma_i^{\text{tot}}$ , used in simulation, for the 10-level system shown in Fig. 2 are given below:

$$\begin{aligned} \Gamma_1^{\text{tot}} &= \Pi \\ \Gamma_2^{\text{tot}} &= \Pi \\ \Gamma_3^{\text{tot}} &= \Pi + \Gamma_{31}^{\text{rad}} + \Gamma_1^{\text{coll}} \\ \Gamma_4^{\text{tot}} &= \Pi + \Gamma_{41}^{\text{rad}} + \Gamma_{42}^{\text{rad}} + \Gamma_1^{\text{coll}} \\ \Gamma_5^{\text{tot}} &= \Pi + \Gamma_{51}^{\text{rad}} + \Gamma_{52}^{\text{rad}} + \Gamma_1^{\text{coll}} \\ \Gamma_6^{\text{tot}} &= \Pi + \Gamma_{62}^{\text{rad}} + \Gamma_1^{\text{coll}} \\ \Gamma_7^{\text{tot}} &= \Pi + \Gamma_{71}^{\text{rad}} + \Gamma_2^{\text{coll}} \\ \Gamma_8^{\text{tot}} &= \Pi + \Gamma_{81}^{\text{rad}} + \Gamma_{82}^{\text{rad}} + \Gamma_2^{\text{coll}} \\ \Gamma_9^{\text{tot}} &= \Pi + \Gamma_{91}^{\text{rad}} + \Gamma_{92}^{\text{rad}} + \Gamma_2^{\text{coll}} \\ \Gamma_{10}^{\text{tot}} &= \Pi + \Gamma_{102}^{\text{rad}} + \Gamma_2^{\text{coll}} \end{aligned} \quad (2)$$

The radiative decay rates are set to  $\Gamma_{31}^{\text{rad}} = \Gamma_{62}^{\text{rad}} = 6$  MHz,  $\Gamma_{41}^{\text{rad}} = \Gamma_{42}^{\text{rad}} = \Gamma_{51}^{\text{rad}} = \Gamma_{52}^{\text{rad}} = 3$  MHz in the case of  $5^2\text{P}_{3/2}(F_e) \rightarrow 5^2\text{S}_{1/2}(F_g)$  hyperfine transitions [19] and  $\Gamma_{71}^{\text{rad}} = \Gamma_{102}^{\text{rad}} = 1.3$  MHz,  $\Gamma_{81}^{\text{rad}} = \Gamma_{82}^{\text{rad}} = \Gamma_{91}^{\text{rad}} = \Gamma_{92}^{\text{rad}} = 0.65$  MHz in the case of  $6^2\text{P}_{3/2}(F_e) \rightarrow 5^2\text{S}_{1/2}(F_g)$  hyperfine transitions [21].  $\Gamma_1^{\text{coll}}$  and  $\Gamma_2^{\text{coll}}$  are  $5^2\text{P}_{3/2}$  and  $6^2\text{P}_{3/2}$  elastic collision decay rates. They are deduced from the experimental values for the self broadening of Rb resonance lines [22]. In our case, their values are about 30 MHz and 24 MHz for  $5^2\text{P}_{3/2} \rightarrow 5^2\text{S}_{1/2}$  and  $6^2\text{P}_{3/2} \rightarrow 5^2\text{S}_{1/2}$  resonance line, respectively.

The differential equations were solved by invoking steady-state conditions and integrated using a standard fourth-order Runge–Kutta method. The population of the  $i$ th atomic level ( $i = 1, 2, \dots, 10$ ) is given by the diagonal density-matrix element  $\rho_{ii}$ , whereas off-diagonal elements represent the slowly varying envelope of the coherences. The real and imaginary parts of the coherence on particular hyperfine transition are related to the refractive index and

the absorption, respectively. The probe absorption line consists of three Doppler broadened hyperfine transitions ( $5^2S_{1/2}(F_g = 2) \rightarrow 6^2P_{3/2}(F_c = 1, 2, 3)$ ). Hence, the total probe absorption is calculated by adding the contributions of the three hyperfine components, i.e., it is equal to  $\text{Im}(\rho_{17}) + \text{Im}(\rho_{18}) + \text{Im}(\rho_{19})$ .

Doppler broadening is taken into account by numerical integration over the velocity distribution. The atomic velocity distribution enters into density matrix equations through the probe and coupling laser detuning  $\Delta_{pi}$  and  $\Delta_{cj}$  defined as

$$\begin{aligned} \Delta_{pi} &= \omega_p - \omega_i - k_p \cdot v_z & i &= 7, 8, 9 \\ \Delta_{cj} &= \omega_c - \omega_j - k_c \cdot v_z & j &= 3, 4, 5 \end{aligned} \quad (3)$$

Here  $\omega_p$  and  $\omega_c$  denote the frequencies of the applied optical fields,  $v_z$  is the atomic velocity along the cell length,  $k_p$  and  $k_c$  are the wave numbers of the applied fields.  $\omega_i$  and  $\omega_j$  are  $5^2S_{1/2}(F_g = 2) \rightarrow 6^2P_{3/2}$  and  $5^2S_{1/2}(F_g = 2) \rightarrow 5^2P_{3/2}$  transition frequencies, respectively.

The coherently induced transparency is driven by the coherence  $\rho_{kl}$  ( $k = 3, \dots, 6$ ;  $l = 7, \dots, 10$ ) on the  $5^2P_{3/2} - 6^2P_{3/2}$  unlinked transitions, which has both real and imaginary components. By changing the coherence decay rates  $\gamma_{kl}$  of the unlinked transitions, the transparency of the medium changes. In Fig. 3, we show the dependence of calculated total probe absorption upon dephasing of the  $5^2P_{3/2} - 6^2P_{3/2}$  unlinked transitions. The calculations were performed for coupling field Rabi frequency of 500 MHz,  $\omega_p = \omega_{17}$  and  $\omega_c = \omega_{14}$ . Total probe absorption is calculated following the density-matrix formalism described above by setting different values for coherence decay rates  $\gamma_{kl}$  of the unlinked transitions. For the  $\gamma_{kl}$  coherence decay rates faster than about 400 MHz the probe absorption remains unchanged. The transparency obtained at this level of coherence decay rates is independent upon the unlinked states coherences and is a result of the ground

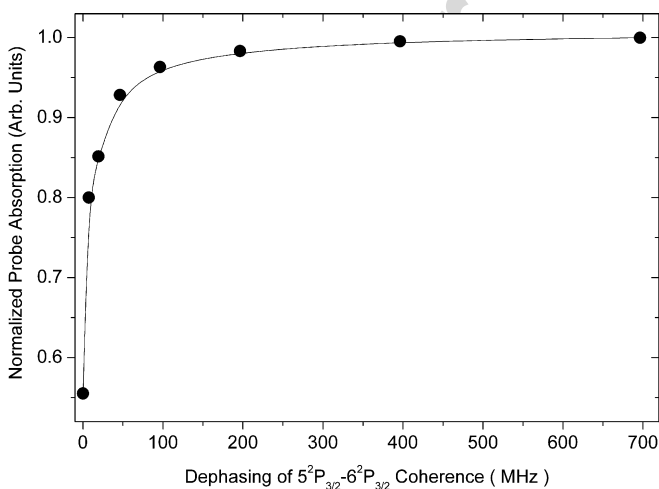


Fig. 3. Total probe absorption (equal to  $-\text{Im}(\rho_{17}) - \text{Im}(\rho_{18}) - \text{Im}(\rho_{19})$ ) with respect to the dephasing of the  $5^2P_{3/2} - 6^2P_{3/2}$  unlinked states coherences. The calculations are performed for coupling field Rabi frequency of 500 MHz,  $\omega_p = \omega_{17}$  and  $\omega_c = \omega_{14}$ .

$5^2S_{1/2}(F_g = 2)$  level population decrease induced by the coupling field saturation effect. In Fig. 3, the total probe absorption is normalized to this value. By decreasing the unlinked coherence decay rates below 100 MHz, a strong dependence on the value of coherence dephasing is observed. An ideal coherence exists and it creates maximum transparency. It is obtained by setting the total coherence decay rates of the unlinked transitions equal to zero (infinite coherence time of unlinked transitions). In our experiment, the coherently induced transparency maximum reaches about 50% of the value determined with coupling field saturation mechanism only.

In Fig. 4, we present calculated probe absorption line profiles for different values of unlinked states coherences and the experimental trace, Fig. 4(e). As the unlinked states coherence decay increases, the EIT window changes in intensity and shape.  $\gamma_{kl}$  coherence decay rate of 46.3 MHz corresponds to the value calculated according to relations (1) and (2). An interesting shape of the EIT window is obtained for zero coherence decay. It consists of numerous

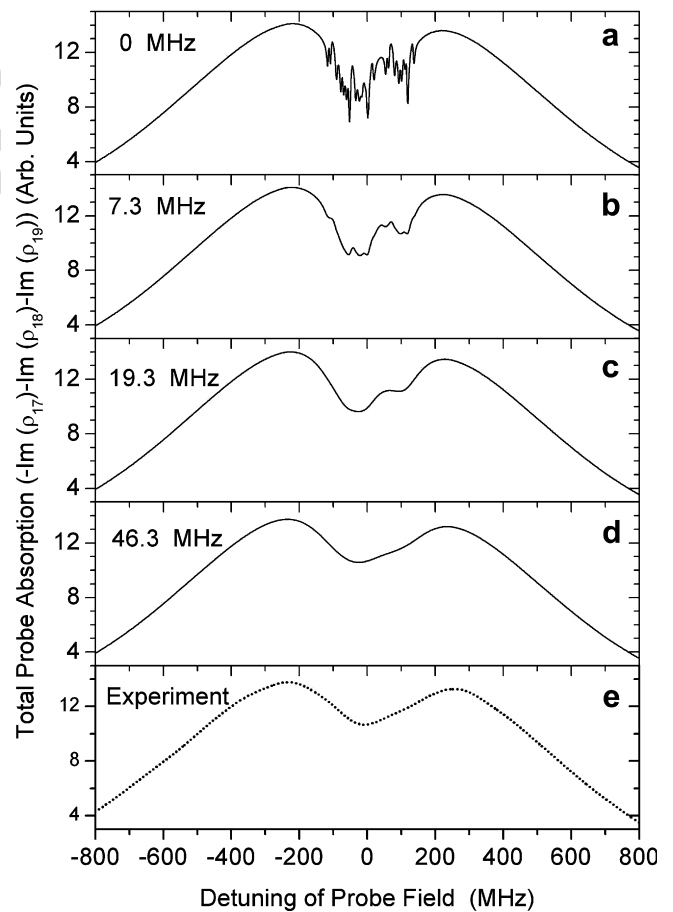


Fig. 4. (a)–(d) Calculated  $5^2S_{1/2}(F_g = 2) \rightarrow 6^2P_{3/2}(F_c = 1, 2, 3)$  Doppler broadened probe absorption line profiles for different values of  $5^2P_{3/2} - 6^2P_{3/2}$  unlinked states coherence decay rates (e) experimental trace for the coupling field power of 35 mW at  $^{85}\text{Rb}$   $5^2S_{1/2}(F_g = 2) \rightarrow 5^2P_{3/2}(F_c = 2)$  transition that should be compared with the calculated profile in (d) case.

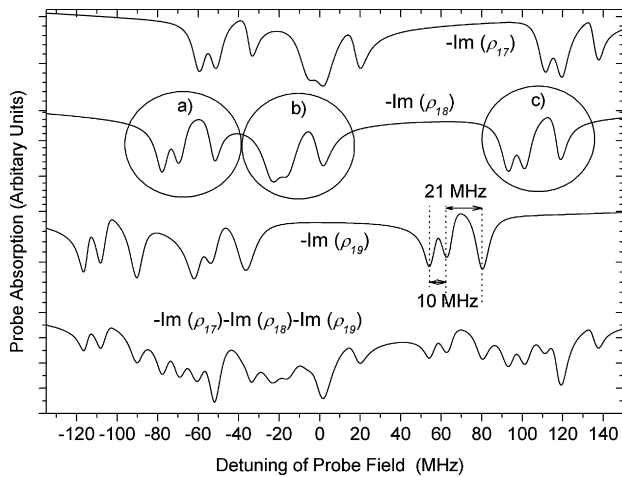


Fig. 5. Detailed view of the calculated probe absorption line profile in the case of ideal coherence. The contributions of each  $5^2S_{1/2}(F_g = 2) \rightarrow 6^2P_{3/2}(F_g = 1, 2, 3)$  hyperfine line forming corresponding probe absorption line are shown. Regarding one hyperfine line there are nine EIT resonances which comes as a result of the  $5^2P_{3/2}$  and  $6^2P_{3/2}$  hyperfine splittings.

sharp EIT resonances. The interpretation of these sharp EIT resonances is clearly seen by inspection of Fig. 5 in which the contributions of each hyperfine line forming the probe absorption line are given. For a given hyperfine transition there are nine EIT resonances resulting from the  $5^2P_{3/2}$  and  $6^2P_{3/2}$  hyperfine structure. In a Doppler broadened medium the atomic transition frequency  $\omega_{ge}$  must be replaced with  $\omega'_{ge} = \omega_{ge} + \vec{k} \cdot \vec{v}$ , where  $\vec{k}$  is the laser wavevector and  $\vec{v}$  is the atomic velocity. Different velocity groups correspond to different detunings  $\delta = \vec{k} \cdot \vec{v}$  of the probe and coupling laser fields and therefore all nine EIT resonances can be obtained. Three group of resonances

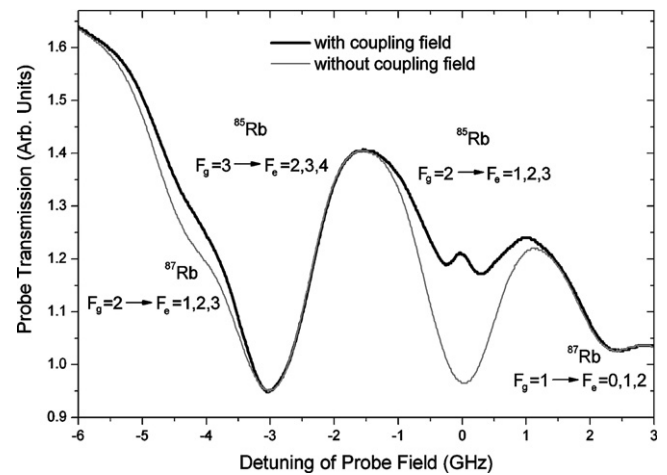


Fig. 6. The experimental traces of the probe field absorption with and without coupling laser. The coupling field power equals to 35 mW and is tuned to the  $^{85}\text{Rb } 5^2S_{1/2}(F_g = 2) \rightarrow 5^2P_{3/2}(F_c = 2)$  transition.

denoted with (a), (b) and (c) correspond to the velocity groups for which the coupling laser is resonant with  $5^2S_{1/2}(F_g = 2) \rightarrow 5^2P_{3/2}(F_c = 1, 2, 3)$  transitions, respectively. Three resonances in each group (a), (b) and (c) reflect the  $6^2P_{3/2}$  hyperfine structure.

#### 4. Experimental results

The experimental traces of the probe field absorption with and without coupling laser are shown in Fig. 6. Two pairs of hyperfine lines corresponding to each rubidium isotope are the result of the hyperfine splitting of the Rb ground  $5^2S_{1/2}$  state, which is 3036 MHz for  $^{85}\text{Rb}$  and 6835 MHz for  $^{87}\text{Rb}$ . The hyperfine lines resulting from

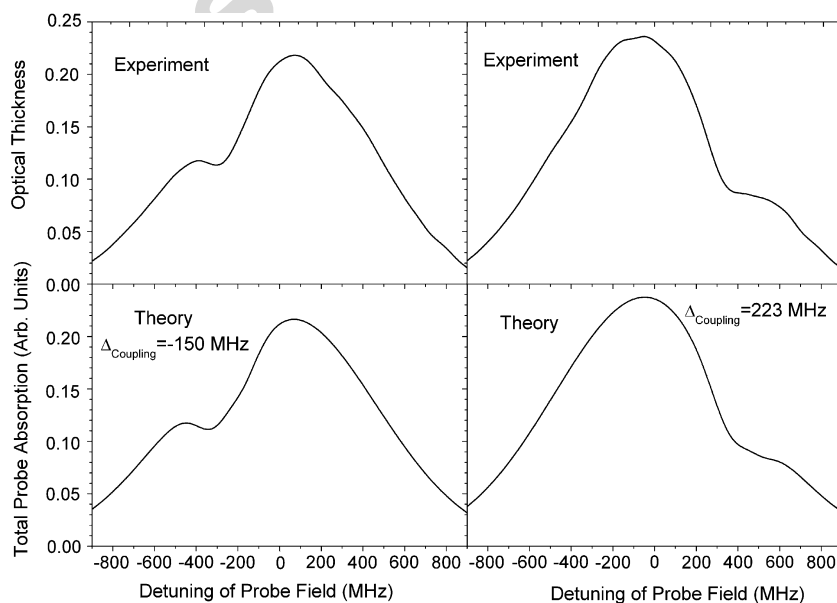


Fig. 7. The effect of coupling laser frequency detuning from  $^{85}\text{Rb } 5^2S_{1/2}(F_g = 2) \rightarrow 5^2P_{3/2}(F_c = 2)$  transition on  $5^2S_{1/2}(F_g = 2) \rightarrow 6^2P_{3/2}(F_c = 1, 2, 3)$  line profile, measurements and theory.

the splitting of the upper  $6^2P_{3/2}$  state are not resolved due to Doppler broadening, which amounts (for the composite line shape) about 1086 MHz (FWHM) at 110 °C. The coupling laser field is in resonance with the  $^{85}\text{Rb } 5^2S_{1/2}(F_g = 2) \rightarrow 5^2P_{3/2}(F_e = 2)$  transition. When the coupling laser is turned on, 67% of the absorption in the centre of the  $5^2S_{1/2}(F_g = 2) \rightarrow 6^2P_{3/2}(F_e = 1, 2, 3)$  line is removed. The absence of optical pumping effects caused by the coupling field is indicated by the lack of corresponding increase in the  $5^2S_{1/2}(F_g = 3) \rightarrow 6^2P_{3/2}(F_e = 2, 3, 4)$  absorption.

In Fig. 4(d) and (e) a comparison between the experiment and theory for  $5^2S_{1/2}(F_g = 2) \rightarrow 6^2P_{3/2}(F_e = 1, 2, 3)$  Doppler broadened line profile at coupling field power of 35 mW and unlinked dephasing coherences of 46.3 MHz can be done. From the discussion given above, it is clear that the decrease of the absorption is predominately due to the coupling field saturation mechanism. Nevertheless, about 8% of the absorption decrease is a result of the coherent effect between unlinked  $5^2P_{3/2}$  and  $6^2P_{3/2}$  states – electromagnetically induced transparency.

The effect of coupling laser frequency detuning from  $^{85}\text{Rb } 5^2S_{1/2}(F_g = 2) \rightarrow 5^2P_{3/2}(F_e = 2)$  transition on  $5^2S_{1/2}(F_g = 2) \rightarrow 6^2P_{3/2}(F_e = 1, 2, 3)$  line profile is shown in Fig. 7. The transparency window shifts following the coupling laser field detuning. In the same figure, the theoretical simulations of the probe absorption for the coupling field detuning of –150 MHz and 223 MHz resemble the experimentally measured profiles.

## 5. Discussion

Several complex physical mechanisms are involved in a real experiment, which mask the EIT signal. There are two major mechanisms which mask the EIT signal in the V-type configuration. The first one is optical pumping between the hyperfine ground-state levels. In our experiment, we suppress this mechanism by heating the rubidium cell. In this way, the thermalization of the ground-state hyperfine level populations is faster than one optical pumping cycle. The second mechanism is coupling field saturation. It can never be experimentally resolved from the EIT signal in the V-type systems. Nevertheless, we showed theoretically how these two effects can be distinguished. Coupling field saturation is an incoherent effect, so the transparency induced by this mechanism does not depend upon the value of coherence between the  $5^2P_{3/2}$ – $6^2P_{3/2}$  unlinked states. This transparency is determined only by the coupling field strength, which remains constant in EIT experiments. On the other hand, EIT is a coherent effect and the induced transparency is strongly dependent upon the unlinked states coherence. The maximum transparency would be obtained in the case of ideal coherence between unlinked states.

Due to the requirement of strong coupling field for the transparency to be observed another effect cannot be ignored, namely the Autler–Townes splitting of the lower

coupled level. This splitting produces the hole in the probe field absorption profile that is enhanced by the EIT window. If the dephasing on the unlinked transition is not sufficiently small, then the Autler–Townes splitting is observed and not EIT. Fortunately, in the V-scheme the transparency that is induced at line center can still be observed in the normal way, because the secondary Autler–Townes components associated with the high-velocity groups that overlap with line center are very small in magnitude [13].

In our previous work the coherent accumulation process through the excitation by a train of the fs pulses has been demonstrated [23,24]. A recent work [25] on coherent effects describes the observation of the electromagnetically induced transparency in rubidium prepared by a comb of optical pulses produced by a cw mode-locked diode laser. The authors proposed possible applications in magnetometry [26], atomic clocks [27] and frequency chains [28]. We are currently working on the coherently induced transparency in the rubidium Doppler-broadened mismatched V-type system by using a femtosecond mode-locked laser as a coupling laser. We find this experiment challenging and expect that it could provide interesting prospect regarding the coherent effects in atomic systems.

## 6. Conclusions

We have observed induced transparency on a blue probe light in a Doppler broadened mismatched V-type system using a low power near infrared coupling laser. Measured transparency on the  $^{85}\text{Rb } 5^2S_{1/2}(F_g = 2) \rightarrow 6^2P_{3/2}(F_e = 1, 2, 3)$  transition shows 67% reduction of absorption in the peak of the Doppler broadened line profile.

Using the extended theoretical modeling of the 10-level  $^{85}\text{Rb}$  atoms with included Doppler broadening we are able to simulate the experimental results. The dependence of the induced EIT window in the  $^{85}\text{Rb } F_g = 2 \rightarrow F_e = 1, 2, 3$  absorption line profile on  $5^2P_{3/2}$ – $6^2P_{3/2}$  unlinked states coherence was analyzed theoretically. In this way it was possible to separate two main mechanisms responsible for the reduction of the absorption in the V-type system: electromagnetically induced transparency and coupling field saturation. We conclude that the observed transparency was predominantly a result of the coupling field saturation mechanism. There is about 8% of the cancellation of absorption via quantum interference due to coherently prepared rubidium atoms.

The results presented in this paper show that a high level of transparency can be obtained even with low power coupling diode lasers. It may provide new insights in the high-frequency inversionless laser technology [15] and possibly simplify its practical realization. This might add a new option in obtaining violet laser action at 420 nm beside that recently published in Ref. [29].

## Acknowledgements

We acknowledge the support from the Ministry of Science, Education and Sports of Republic of Croatia (Projects 0035002), European Commission Research Training Network (FW-5) and Alexander von Humboldt Foundation, (Germany).

## References

- [1] S.E. Harris, *Phys. Today* 50 (1997) 36.
- [2] A. André, M.D. Eisaman, R.L. Walsworth, A.S. Zibrov, M.D. Lukin, *J. Phys. B: At. Mol. Opt.* 38 (2005) S589.
- [3] A. Imamoglu, S.E. Harris, *Opt. Lett.* 14 (1989) 1344.
- [4] K.J. Boller, A. Imamoglu, S.E. Harris, *Phys. Rev. Lett.* 66 (1991) 2593.
- [5] O. Kocharovskaya, *Phys. Rep.* 219 (1992) 175.
- [6] W.E. van der Veer, R.J.J. van Diest, A. Dönszelmann, H.B. van Linden van der Heuvell, *Phys. Rev. Lett.* 70 (1993) 3243.
- [7] M. Fleischhauer, A. Imamoglu, J.P. Marangos, *Rev. Mod. Phys.* 77 (2005) 633.
- [8] S.E. Harris, J.E. Field, A. Imamoglu, *Phys. Rev. Lett.* 64 (1990) 1107.
- [9] M.D. Lukin, *Rev. Mod. Phys.* 75 (2003) 457.
- [10] D. McGloin, M.H. Dunn, D.J. Fulton, *Phys. Rev. A* 62 (2000) 053802.
- [11] G.G. Padmabandu, G.R. Welch, I.N. Shubin, E.S. Fry, D.E. Nikonov, M.D. Lukin, M.O. Scully, *Phys. Rev. Lett.* 76 (1996) 2053.
- [12] A.S. Zibrov, M.D. Lukin, D.E. Nikonov, L. Hollberg, M.O. Scully, V.L. Velichansky, H.G. Robinson, *Phys. Rev. Lett.* 75 (1995) 1499.
- [13] J.R. Boon, E. Zekou, D. McGloin, M.H. Dunn, *Phys. Rev. A* 59 (1999) 4675.
- [14] D.J. Fulton, S. Shepherd, R.R. Moseley, B.D. Sinclair, M.H. Dunn, *Phys. Rev. A* 52 (1995) 2302.
- [15] J.R. Boon, E. Zekou, D.J. Fulton, M.H. Dunn, *Phys. Rev. A* 57 (1998) 1323.
- [16] M.D. Lukin, M.O. Scully, G.R. Welch, E.S. Fry, L. Hollberg, G.G. Padmabandu, H.G. Robinson, A.S. Zibrov, *Laser Phys.* 6,436 (1996).
- [17] Y. Li, M. Xiao, *Phys. Rev. A* 51 (1995) R2703.
- [18] K.B. MacAdam, A. Steinbach, C. Wieman, *Am. J. Phys.* 60 (1992) 1098.
- [19] D.A. Steck, Rubidium 87 D Line Data, <http://steck.us/alkalidata>.
- [20] C. Cohen-Tannoudji, A. Kastler, *Prog. Opt.* 5 (1966) 3.
- [21] E. Gomez, S. Aubin, L.A. Orozco, G.D. Sprouse, *J. Opt. Soc. Am. B* 21 (2004) 2058.
- [22] W. Demtröder, *Laser Spectroscopy*, Springer-Verlag, Berlin, 2003.
- [23] D. Aumiler, T. Ban, H. Skenderović, G. Pichler, *Phys. Rev. Lett.* 95 (2005) 233001.
- [24] T. Ban, D. Aumiler, H. Skenderović, G. Pichler, *Phys. Rev. A* 73 (2006) 043407.
- [25] V.A. Sautenkov, Y.V. Rostovtsev, C.Y. Ye, G.R. Welch, O. Kocharovskaya, M.O. Scully, *Phys. Rev. A* 71 (2005) 063804.
- [26] M.O. Scully, *Phys. Rev. Lett.* 67 (1991) 1855.
- [27] S.A. Diddams, Th. Udem, J.C. Bergquist, E.A. Curtis, R.E. Drullinger, L. Hollberg, W.M. Itano, W.D. Lee, C.W. Oates, K.R. Vogel, D.J. Wineland, *Science* 293 (2001) 825.
- [28] S.A. Diddams, D.J. Jones, J. Ye, S.T. Cundiff, J.L. Hall, *Phys. Rev. Lett.* 84 (2000) 5102.
- [29] T. Meijer, J.D. White, B. Smeets, M. Jeppesen, R.E. Scholten, *Opt. Lett.* 31 (2006) 1002.